Experimental Study on Low Voltage Ride-Through of DFIG-Based Wind Turbine

Ngo Minh Khoa[1], Doan Duc Tung[1], and Le Van Dai[2]
[1] Faculty of Engineering and Technology, Quy Nhon University, Quy Nhon City, Binh Dinh, Vietnam
[2] Faculty of Electrical Engineering Technology, Industrial University of Ho Chi Minh City, Ho Chi Minh, Vietnam
Email: {ngominhkhoa; doanductung}@qnu.edu.vn; levandai@iuh.edu.vn

***Abstract*—This paper presents an architecture of the Doubly-Fed Induction Generator based on Wind Energy Conversion System (DFIG-WECS) to study with the Low Voltage Ride Through (LVRT) capability. The proposed architecture consists of three main parts namely the wind turbine, electric generator, control systems. The wind turbine and gearbox are modeled by a servo motor driven by using an inverter system. The electric generator uses the Wound Rotor Induction Generator (WRIG). The control system composes of the rotor-side converter (RSC) and the grid-side converter (GSC). The integration of the digital signal processor (DSP) with the Simulink/Matlab software of the vector control scheme is implemented to control both RSC and GSC. Besides, to protect the overcurrent of the generator's rotor and overvoltage of the DC-link, the crowbar and chopper circuits and the logical scheme between the crowbar and the RSC are also proposed. To approve the control algorithms implemented in DSP as hardware in the loops, the proposed 0.8kW DFIG-WESC system has been performed under the experimental environment considering LVRT requirement in German grid code.**

***Index Terms*—DFIG, LVRT, DSP, wind turbine, grid-connected code**

I. Introduction

Wind power technologies and applications have been significantly developed for the past ten years. Wind power is now a vital renewable energy resource. Its characteristic is to gather the wind's kinetic energy, convert it into electric power, and finally transfer the power into the power system [1], [2]. The electric-wind generation structure consists of six main parts such as wind turbine, gearbox, generator, power converter, and step-up transformer. In recent years, variable-speed wind turbine systems have become more popular because of energy-harvesting capability, flexibility adaptability, reliability, etc. The variable-speed wind turbine systems based on Synchronous Generator (SG) and Doubly-Fed Induction Generator (DFIG) are the two most well-known configurations [3]–[7]. Besides, the comparison between three types of generators in Wind Energy Conversion Systems (WECS) including self-excited induction generator, doubly-fed induction generator, and switched reluctance generators are presented in [8]. For three types of generators in WECS, because of developments of power electronics devices, the DFIG can properly operate at a large range of wind speed with improvement the voltage sensitivity. Nowadays, the DFIG is widely applied in the market and it is the study object in this paper.

For the wind power system, the grid codes are rules for the system to be coupled with the network. The grid codes are established by the power system operation experts to make flat the impacts of large-scale wind power plants on the stability of power system stability [9]. One of the key goals of wind turbine manufacturers is to design accordant control and protection strategies to fulfill the grid codes. In this work, the grid code namely Low Voltage Ride Through (LVRT) to maintain the connection of the wind power generation system to the grid under the voltage dip conditions is studied by an experimental approach. Several works related to the LVRT capability of the DFIG have been reported in the literature. As presented in [10], more than 190 research works about LVRT problems and available techniques to integrate wind energy systems into the power grid have been studied. The authors in [10] comprehensively reviewed the literature concerning the enhancement approaches of the LVRT capability of DFIG-based wind turbines. The authors in [11] proposed an approach based on limiting the high rotor current of the DFIG to save the converter and to make a bypass for this current through resistors that are linked to the rotor windings. Besides, the approach can control for supporting reactive power to the power grid during long dips for facilitating voltage restoration. The voltage recovery of DFIG-based wind turbines was investigated in [12], as well as a new control method was proposed for re-establishing the terminal voltage of the DFIG after an external fault in the power grid is cleared. The behavior of the DFIG-based wind turbines under unbalanced voltage conditions at the grid-side [13], three-phase voltage dips [14] was studied using simulations. The dynamic response of the rotor-side converter during faults on power systems was investigated in [15], [16].

Much research interest in developing novel approach methodologies was studied for the purpose of improving the performance of the LVRT capability of DFIG-based wind turbines [17]–[27]. The majority of the control methodologies presented in the literature concerns [17].

Manuscript received June 7, 2021; revised July 25, 2021; accepted August 16, 2021.
Corresponding author: Le Van Dai (email: levandai@iuh.edu.vn).

An effective scheme for improving the LVRT capability of DFIG-based wind turbines when unbalanced voltage dip conditions occurred at the grid-side was proposed in [18]. It was used by jointing the application of the rotor-side converter control and a three-phase stator damping resistor which is located in series with the windings of the stator. Its performance was to limit the maximum inrush current values in the rotor windings, electromagnetic torque, and DFIG transient response at the times of starting and ending the fault. In [19], a series crowbar resistance with an Insulated Gate Bipolar Transistor (IGBT) was proposed to improve the LVRT competency of DFIG driven grid-integrated Wind Energy Conversion Systems (WECS). The authors in Ref. [20] proposed an intelligent Fault Ride-Through (FRT) strategy for DFIG-based WECS to control active power and reactive power during grid faults. In the strategy, a wind speed estimation process is based on the fuzzy method in the operation mode of Maximum Power Point Tracking (MPPT) under normal conditions and a hybrid genetic algorithm based on the real and reactive controller with a DC-chopper. Fuzzy control for double resistors braking method was proposed in [21] for improving the performance of the LVRT of DFIG. Liu *et al*. in [22] proposed an LVRT control to improve the small-signal stability of the DFIG-based wind turbines during fault conditions. The authors in [23] designed a new protection system of the crowbar for enhancing the LVRT capability of DFIG. For improving the performance of steady-state and dynamic modes under different operating conditions of DFIG-based wind energy converter system, the works in Refs [24], [25] proposed feasible control strategies in which the rotor-side control scheme was developed on the model predictive control. Mosaad *et al*. proposed a model-free adaptive control for a unified power flow controller to enhance the dynamic performance of fault ride through capability of the DFIG under different voltage disturbances [26] and developed a new cost-effective technique for improving the LVRT capability of the DFIG system based on the integration of high-temperature superconductor within the DC link of the rotor-side and grid-side converters [27].

Experimental research on the LVRT capability of DFIG has been studied in the literature [28]–[32]. In Ref. [28], the experimental setup test was carried out on a 10kW experimental system, dip generator was applied for creating grid voltage dips up to 20% of rated voltage with different duration times. The experimental FRT performance of a 250kW brushless DFIG was studied in [29] where a control strategy was implemented on a prototype 250kW brushless DFIG. The authors in Ref. [30] proposed a demagnetization current controller for enhancing the FRT capability. The authors in [31] proposed the dynamic voltage and current assignment topologies for the DFIG system. These strategies were implemented and verified in experimental results of the 1.5kW DFIG system. In [32], a ride-through simulation study of a 2 MW DFIG under a short-term unsymmetrical network disturbance was presented.

This paper presents a configuration of DFIG wind turbines for the experimental study on LVRT capability in our university's laboratory. The vector control based on pulse width modulation (PWM) is introduced for both RSC and GSC. The proportional-integral (PI) controller is chosen as the control strategy and the AC-crowbar and DC-chopper are the protection circuits. The experiment of the proposed configuration of DFIG wind turbines under the balanced and unbalanced voltage dip condition tests is carried out to analyze and validate the LVRT requirement in the German grid code.

The main contributions of this work include: (*i*) The integration of the digital signal processor (DSP) with the Simulink/ Matlab software of the vector control scheme, (ii) The suggested observer approach is realized with the help of the TMS320F28335 DSP, (iii) the complete architecture of DFIG-WECS to study with LVRT capability.

The remains of this paper are organized as follows. The configuration and modeling of the DFIG test system are introduced in Section II. Section III points to the control scheme of the DFIG test system. The main contents involving the experimental setup are given in Section IV. Section V analyzes the experimental results. Finally, the conclusions are shown in Section VI.

II. Model Configuration

The configuration of a DFIG-based wind turbine system is proposed in this study as shown in Fig. 1. This configuration composes of main parts such as the wind turbine, rotor-side converter (RSC), grid-side converter (GSC), DC-chopper, and AC- crowbar. Especially, for the experimental system, the wind turbine and gearbox are replaced by the servo motor. To create a fault in the network, a grid emulator is used in the testing workbench. The DFIG system and its converters in the testing workbench is a small-scale power system, which means the power rating of the DFIG, the RSC, and the GSC in the testing workbench will be much smaller than the practical system [7].

A. Wind Turbine Model

The wind turbine and gearbox are modeled by a servo motor that is driven by using an inverter system. Therefore, the mechanical response of the wind turbine and gearbox will be emulated by the servo motor drive system. The mechanical power from the servo motor can be transferred to the generator of DFIG via their mechanical shaft, so the DFIG system can generate power for supplying to the grid. Its model is established to satisfy the mathematical equations as follows.

The aerodynamic torque is:

$$T_m = P_m / \omega_t \tag{1}$$

The mechanical power is:

$$P_m = \frac{1}{2}\rho S C_P(\lambda, \beta) v_{\text{wind}}^3 \tag{2}$$

in which ω_t is the mechanical speed, ρ is the air density, S is the blade swept area, $C_p(\cdot)$ is the performance coefficient, λ is the tip speed ratio, β is the blade pitch angle, and v_{wind} is the wind speed.

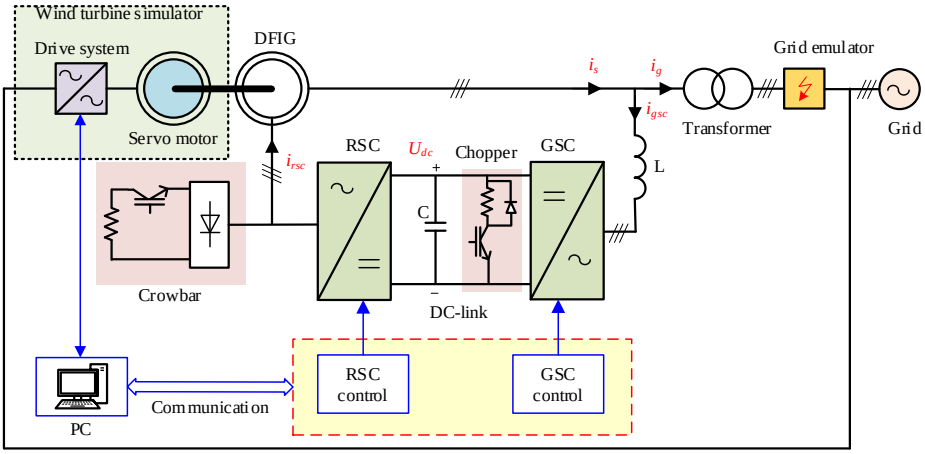

Fig. 1. The proposed DFIG-wind turbine system.

B. Generator Model

The electric generator used in this case is a wound rotor induction generator (WRIG) with the stator winding and the rotor winding. Its model is established in the *d-q* reference frame to satisfy the following mathematical equations [24]:

The voltage equations:

$$\begin{aligned} u_{sd} &= R_s i_{sd} - \omega_s \lambda_{sq} + \frac{d}{dt}\lambda_{sd} \\ u_{sq} &= R_s i_{sq} + \omega_s \lambda_{sd} + \frac{d}{dt}\lambda_{sq} \\ u_{rd} &= R_r i_{rd} - (\omega_s - \omega_r)\lambda_{rq} + \frac{d}{dt}\lambda_{rd} \\ u_{rq} &= R_r i_{rq} + (\omega_s - \omega_r)\lambda_{rd} + \frac{d}{dt}\lambda_{rq} \end{aligned} \tag{3}$$

in which subscripts *s* and *r* express the stator and rotor quanta, respectively. Subscripts *d* and *q* express for the *d*- and *q*-axis components, respectively; ω_s is the electrical angular speed of the grid voltage; *R* is the resistance; *u*, *i* and λ are the voltage, current, and flux, respectively; $\omega_r = n_p\omega_m$ is the rotor angular frequency, where ω_m is rotor mechanical speed and n_p is the number of pole pairs.

The flux equations:

$$\begin{aligned} \lambda_{sd} &= (L_{ls} + L_m)i_{sd} + L_m i_{rd} = L_s i_{sd} + L_m i_{rd} \\ \lambda_{sq} &= (L_{ls} + L_m)i_{sq} + L_m i_{rq} = L_s i_{sq} + L_m i_{rq} \\ \lambda_{rd} &= (L_{lr} + L_m)i_{rd} + L_m i_{sd} = L_r i_{rd} + L_m i_{sd} \\ \lambda_{rq} &= (L_{lr} + L_m)i_{rq} + L_m i_{sq} = L_r i_{rq} + L_m i_{sq} \end{aligned} \tag{4}$$

where *L*, L_l, and L_m are self-inductance, leakage inductance, and mutual inductance, respectively.

The electromagnetic torque equation:

$$T_{em} = \frac{3}{2} n_p (i_{sq}\lambda_{sd} - i_{sd}\lambda_{sq}) \tag{5}$$

The instantaneous stator and rotor active power equations [33].

$$\begin{aligned} P_s &= -\frac{3}{2}\omega_s \left(\lambda_{sq} i_{sd} - \lambda_{sd} i_{sq}\right) \\ P_r &= -\frac{3}{2}\left(\omega_s - \omega_r\right)\left(\lambda_{rq} i_{rd} - \lambda_{rd} i_{rq}\right) \end{aligned} \tag{6}$$

C. Protection Circuit

As shown in Fig. 1, the protection circuit has two protection circuits including a crowbar and a chopper. Using the chopper is to increase the normal operating range of the DFIG-wind turbine when having the power imbalance between the RSC and the GSC and not essential for LVRT. The crowbar circuit is used to protect the RSC due to over-current in the generator rotor windings or over-voltage in the DC-link. After over-current due to the voltage dips is detected, the RSC is immediately blocked, and the crowbar is activated at the same time. When the crowbar is activated, the RSC is separated from the rotor windings.

III. Control Scheme

The vector control base on the PWM is introduced for both the RSC and the GSC. The proportional-integral (PI) control is chosen as the control strategy. For easier controller design, the AC phase variables are transferred into the DC variables. The detailed transformation process has been referred to [34]. For PI control, the selection of control parameters is very essential to make good performance although the entire system might be able to operate with a wide range of the parameters. The Butterworth polynomial applied to optimize the closed-loop eigenvalue locations, which has been introduced in [35] and re-applied in [36], is used in this study.

A. Grid-Side Converter Control

The control target of GSC is to provide a constant DC-link voltage for the RSC and to provide reactive support to the grid if required. Besides, the GSC can receive or deliver active power according to the DFIG operating mode. Therefore, the main tasks of the GSC conclude: to control the power flow between the GSC and the grid; to regulate the DC-link voltage for the RSC [7]. The GSC control scheme in this testing workbench is shown in Fig. 2. The three-phase grid voltage u_g, the three-phase grid current i_g, and the DC-link voltage U_{dc} are sampled as inputs of the scheme. The grid angle θ_s and angular speed ω_s are produced by the PLL. The GSC control scheme includes the inner loop for the current and the outer loop for the DC-link voltage/reactive power. The DC-link

voltage reference U_{dc}^{ref} is compared with the sampled DC-link voltage U_{dc}. The difference is as an input of the outer loop proportional-integral (PI) controller, and the rotor current references in *d*-axis i_{dc}^{ref} are the outputs of the PI controller. The control loop of reactive power is an open loop in where the rotor current reference in *d*-axis i_{gq}^{ref} is established. After decoupling, the inner current loop is designed and the grid currents in the *dq* reference frame i_{gd} and i_{gq} can be adjusted by the GSC output voltage u_d and u_q. The controllers based on the PI control approach in the reference frames are applied and the voltage references of the GSC u_d^{ref} and u_q^{ref} are the outputs of the PI controller after decoupling. They are pushed to the *abc* reference frame and the control signals are created after the sinusoidal pulse width modulation (SPWM) [7], [37]–[39].

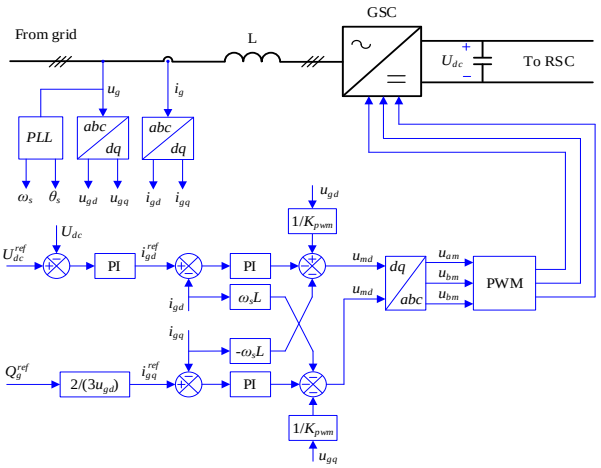

Fig. 2. The control scheme of the grid-side converter (GSC).

The active power and reactive power from the grid to the GSC can be derived from its control scheme as follows:

$$P_g = -\frac{3}{2}\left(v_{gd}i_{gd} + v_{gq}i_{gq}\right)$$
$$Q_s = -\frac{3}{2}\left(v_{gq}i_{gd} - v_{gd}i_{gq}\right) \quad (7)$$

The DC-side equation of the GSC with L filter is derived in the *dq*- frame orientation:

$$C\frac{du_{dc}}{dt} = i_{dc} - \frac{3}{2}\frac{u_s}{u_{dc}}i_{gd} \quad (8)$$

where i_{dc} is the external current flowing into the DC bus of the converter and it can be controlled through the *d*-axis currents i_{gd}.

B. Rotor-Side Converter Control

The RSC is to control and switch the different operating modes of the DFIG including starting mode, speed control mode, and power control mode which depend on various working conditions [37], [39]. Their control strategy of the power control mode is shown in Fig. 3. For the power control mode, after the stator windings of the DFIG are connected to the grid, the DFIG begins to generate power to the grid. The active and reactive power generated by the DFIG carried out by the power commands from the wind turbine center controller. These commands have followed the algorithm to realize maximum power point tracking as well as the operating conditions of the transmission system. Looking at Fig. 3, in the power mode control, the grid synchronization for the RSC is also needed by using a PLL to get the information of grid phase angle θ_s and angular speed ω_s.

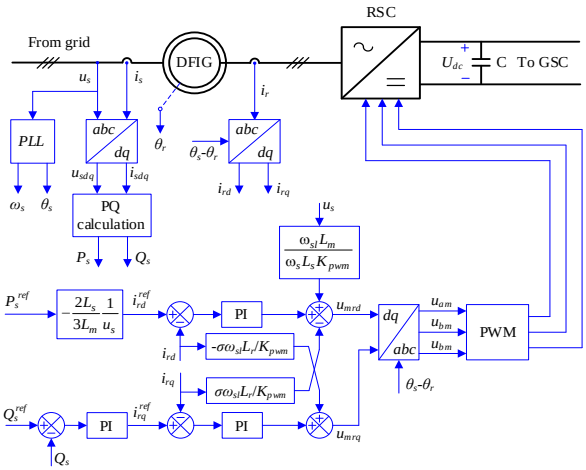

Fig. 3. The control scheme of the rotorside converter (RSC).

From the control scheme of the RSC in Fig. 3, it is observed that the stator output active power P_s depends on the stator *d*-axis current i_{sd} while the stator output reactive power depends on the stator q-axis current i_{sq} [7]. The equations for determining the active and reactive powers are derived as follows:

$$P_s = -\frac{3}{2}\frac{L_m}{L_s}u_s i_{rd}$$
$$Q_s = \frac{3}{2}\frac{u_s^2}{\omega_s L_s} + \frac{3}{2}\frac{L_m}{L_s}u_s i_{rq} \quad (9)$$

C. Method for LVRT Behavior

In the 0.8kW DFIG experimental setup, a crowbar circuit is set up to protect the turbine during the fault period for improving the LVRT capability of the DFIG. The method used for reverberating LVRT of the DFIG system is a set of logical switches between the crowbar and the RSC as shown in Fig. 4. The schematic diagram will operate in one of four operating modes depending on the LVRT condition: Mode #0 is a mode in which the DFIG is normally operated with the power control mode; Mode #1 is a mode in which the crowbar is activated, the RSC is kept at open status, and the PI controllers of the converters are reset; Mode #2 is a mode in which the current control mode is activated during a voltage dip condition, and Mode #3 is a mode in which the RSC control is returned to the power control mode. Therefore, when the protection system detects a fault in the grid, a command to switch on the crowbar and the RSC is kept at open status. At the same time, the rotor current is flowing through the crowbar resistor. In addition, when the crowbar is activated the RSC pulses are disabled and the DFIG behaves like a squirrel cage induction machine directly coupled to the grid.

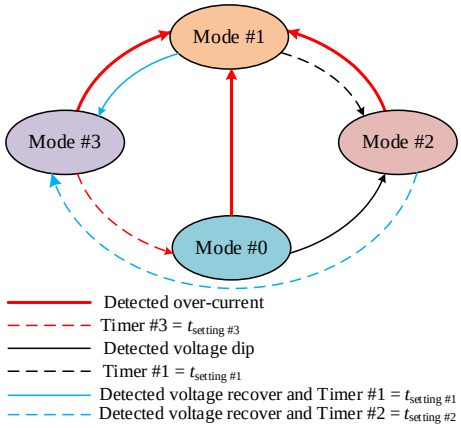

Fig. 4. The logical scheme between the crowbar and the RSC.

IV. Experimental Setup

The overall experimental set-up is shown in Fig. 5. The proposed observer approach is used with the help of the TMS320F28335 DSP as the core CPU of the control system. The LA-55-P Hall-effect current sensors are used to measure the real-time rotor and stator side currents of DFIG-WECS and The LA-55-P Hall-effect voltage sensors are employed to measure the stator and DC-link voltages.

The test system in our university's laboratory is shown in Fig. 5 (a). In the schematic diagram, the wind turbine-gearbox system is modeled by a servo motor and is driven by an inverter unit.

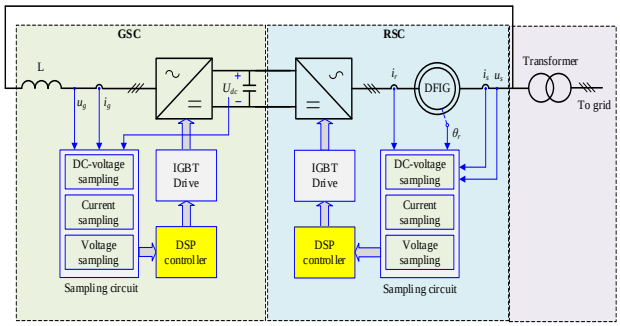

(a)

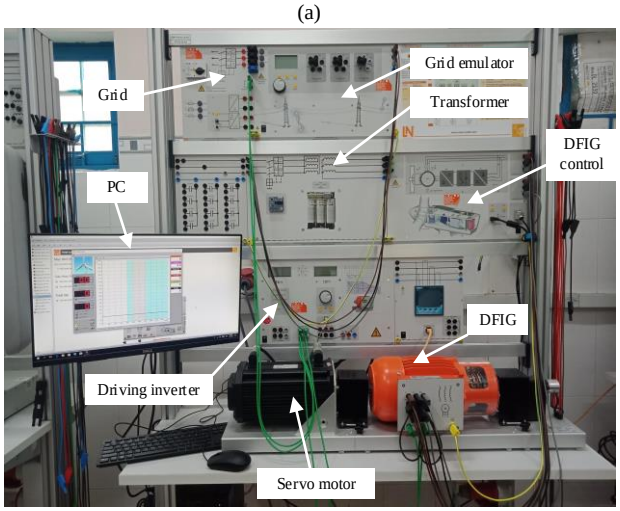

(b)

Fig. 5. The experimental setup: (a) Schematic diagram, (b) The experimental setup for LVRT of DFIG-based wind turbine.

Therefore, its mechanical responses can be easily controlled to emulate a voltage dip, a grid emulator is located at the point common coupling (PCC) as shown in Fig. 1 to create the balanced and unbalanced voltage dips. Moreover, the remaining magnitude and duration of the voltage dips can be varied with different values. The DFIG system and its converters in the testing workbench are small-scale power ratings which are the power rating of the DFIG, the RSC, and the GSC of the testing workbench will be much smaller than the practical DFIG system [7]. For a practical DFIG system, the up-level control signal is normally deriving from the controller of the wind turbine system. However, it can be made by a personal computer linking up with the RSC and the GSC controller for the DFIG testing workbench. The wind turbine in a practical DFIG system is imitated by the servo motor driven via its driving inverter in a DFIG testing workbench. The mechanical power generated by the servo motor can be transferred to the generator of the DFIG system via their shaft, and the DFIG system can then transfer power to the power system. The hardware units of the DFIG testing workbench in the laboratory shown in Fig. 5 (b) consist of the main parts of the DFIG mentioned above.

The main parameters of the DFIG in the testing workbench are presented in Table I. It is clear from Table I that the nominal power of the DFIG is 0.8kW and the nominal voltage of the DFIG is 400V for the star connection or 230V for the delta connection. The nominal speed of the synchronous mode and the asynchronous mode is 1500rpm and 1400rpm, respectively. Based on the hardware units, the authors in this paper have carried out the tests for evaluating the LVRT capability of the DFIG.

TABLE I: Main Parameters of the DFIG in the 0.8kW Testing Workbench

Parameter	Value	Units
Generator		
Nominal voltage (Y/delta)	400/230	V
Nominal current	2/3.5	A
Nominal frequency	50	Hz
Nominal power	0.8	kW
Nominal speed (synchronous/asynchronous)	1500/1400	rpm
cosφ	1/0.75	
Exciter voltage	130~/24=	V
Exciter current	0.4~/11=	A
Momentum of inertia	0.0066	kgm^2
Stator resistance	8	Ω
Stator reactance	17.5	Ω
Rotor resistance	7.3	Ω
Rotor reactance	17.6	Ω
Main reactance	193	Ω
GSC control		
Nominal power	250	VA
Nominal voltage	320	V
Inductance	200	mH
Parasitic resistance	9.3	Ω
DC-link capacitance	110	μF
DC-link voltage	550	V
Switching frequency	10	kHz
RSC control		
Nominal power	250	VA
Nominal voltage	320	V
Switching frequency	10	kHz

A. Grid-Side Converter

The control circuits are designed and developed to realize the control scheme presented above. For the testing workbench, the scheme of the GSC control circuits is shown in Fig. 5. They include three main components [7]: (*i*) *Sampling circuit*: It is used to measure the GSC parameters including the output current, the DC voltage, and grid voltage. In addition, the sampling circuit converts the parameters into the digital signals which are compatible with the digital signal processing (DSP) controller as shown in Fig. 5. Therefore, the sampling circuit consists of three parts: the current sampling, the voltage sampling, and the DC-link voltage sampling circuits. The output of the sampling circuit is feedback in the control loop and the DSP controller. (*ii*) *DSP controller*: It is the main processing unit of the whole system. The related computations in the control scheme have proceeded in the DSP controller. The duty cycles of a switching device are also created in the DSP controller and pushed to the IGBT drive. Moreover, the control signals are sent to the contactor drive by the DSP controller to control the contactor driving. (*iii*) *IGBT drivers*: The DSP controller transmits the duty cycle signals to the IGBT drivers to drive the IGBT switch. In addition, the GSC can create the output voltage which is used by the DSP controller. Therefore, the loop of control can be closed-loop connected.

B. Rotor-Side Converter

The RSC control circuits conclude the main components including the sampling circuit, the DSP controller, and the IGBT driver as shown in Fig. 5. Its control circuits conclude three main parts [7]: (*i*) *Sampling circuit*: The several control variables including the grid voltage, the stator current, the stator voltage, and the rotor current are measured by the sampling circuit and then they are transferred into the digital signals to fit in the DSP controller as shown in Fig. 5. The sampling circuit output is seen as feedback of the control loop and connected to the DSP controller. (*ii*) *DSP controller*: In the RSC, it is also operating as the main processing unit of the system. The related computations in the three operating modes are implemented in the DSP controller. The duty cycles of a switching device are also created in the DSP controller and then they are sent to the IGBT drive. Moreover, the control signals will be sent to the contactor drive by the DSP controller to control the contactor. (*iii*) *IGBT driver*: The duty cycle signals from the DSP controller are sent to the IGBT driver to drive the IGBT. Therefore, the RSC can control the output rotor voltage which is required by the control scheme and the control loop can be closed-loop connected.

V. Experimental Results and Discussion

The DFIG experimental system in the laboratory is a product of Lucas Nuller, Germany. Fig. 6 presents the LVRT testing curve of the state grid of Germany at present considered to validate the LVRT of the DFIG wind turbines. This characteristic shows that if the voltage dip with a remaining voltage magnitude and a time duration is above the characteristic (red line) the DFIG is still connected to the grid for normally operating. Otherwise, the DFIG will be conditionally disconnected permissible [9]–[11].

The center control program is designed and applied in this testing workbench as shown in Fig. 7 (a). From this program, the input variables including the wind speed, wind profile, pitch angle, and control mode can be established by the user. In addition, the output variables such as the rotor speed, torque, and generated active power to the grid can display. All obtained results are displayed and recorded on the monitor as shown in Fig. 7 (b). As shown in Fig. 7 (b), the voltage, current, DC-link voltage waveforms, etc. can be used for analyzing the LVRT capability. Moreover, these experimental results can be also saved under a text file for further analysis.

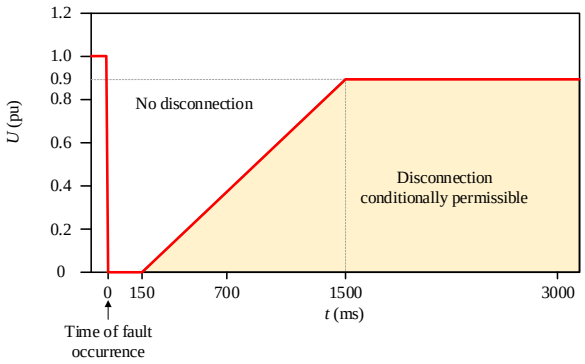

Fig. 6. LVRT requirement in German grid code.

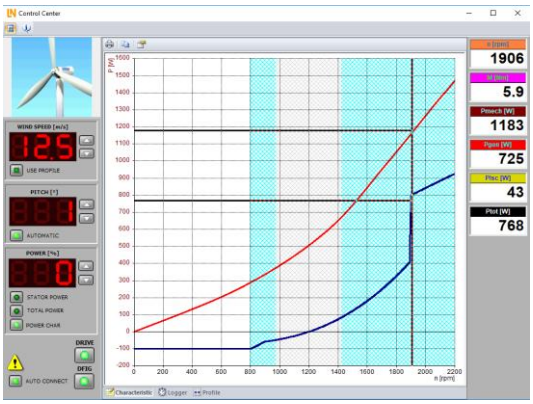

(a)

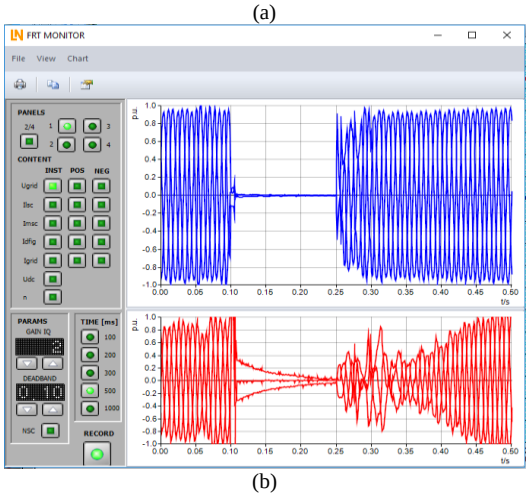

(b)

Fig. 7. (a) The user interface of the control center, (b) Recorded experimental waveforms.

The test system is established as the schematic diagram shown in Fig. 5 (a). The main parameters of the system are listed in Table I. The DFIG is connected to the 380V, 50Hz grid. The wind speed is obtained using the driving motor through the central control on the PC. For all experiments carried out in this paper, the wind speed is kept at 12.5m/s. At the wind speed, the DFIG is generating the output active power of 750W to the grid and the reactive power is set equal to zero in steady-state. A voltage dip is created by using the grid emulator. The grid emulator can create balance voltage dip or unbalance voltage dips which have the remaining voltage magnitude of the phases reduced in a short time. Three voltage dip types, including three-phase to ground fault, single-phase to ground fault, and phase-to-phase fault, are considered for this study by applying the grid emulator. Moreover, the remaining voltage magnitude and the time duration of the voltage dips can be adjusted for suiting the purpose.

The DFIG generator is driven by a servo motor at a constant speed. The wind speed is set to be constant at 12.5m/s, at which condition the DFIG generates 750W output active power. Other parameters of the DFIG system in steady-state are set on the graphical by the user as shown in Fig. 7 (a). Experiments have been carried out with two condition tests that are balanced and unbalanced voltage dip.

A. Test Under Balanced Voltage Dip Condition

Fig. 8 shows a three-phase voltage dip due to a three-phase to ground fault with 100% of nominal voltage at the PCC side by using the grid emulator happens at a time duration of 150ms starting 50ms. Three-phase RMS voltage u_g at the PCC is recorded as shown in Fig. 8 (a). Observing that the pre-fault stage from zero to 100ms, the three-phase RMS voltage u_g is normal with a magnitude of around 1.0pu. At the time of 100ms, the fault happens, so the three-phase voltage magnitudes u_g are reduced to zero within the period from 100ms to 250ms. The grid voltage u_g is recovered at the time of 250ms. In addition, the three-phase RMS current of the grid-side is displayed and recorded for evaluating the LVRT capability of the DFIG testing workbench as shown in Fig. 8 (b). It is clearly that in the pre-fault stage from zero to 100ms, the three-phase grid currents i_g are normal at around the nominal current of 1.0pu. However, at the time that the fault is started, the three-phase grid currents i_g are sharply increased and then they are gradually decreased to zero. At the time of 250ms, the grid voltage u_g is recovered, three-phase grid currents i_g have also come back to the nominal values as the pre-fault stage. Besides, the stator current i_s, the GSC current i_{gsc}, the RSC current i_{rsc}, and the DC-link voltage U_{dc} are shown in Fig. 8 (c), Fig. 8 (d), Fig. 8 (e), and Fig. 8 (f), respectively. The *d*- and *q*-components of those currents are used in this case to see the effectiveness of the DFIG controllers. At the fault time from 100ms to 250ms, the DC-link voltage U_{dc} as shown in Fig. 8 (f) is slightly decreased but the GSC and the RSC controllers are normally operated, and it can see in Fig. 8 (c), Fig. 8 (d), and Fig. 8 (e). The active power and reactive power generated by the DFIG to the grid is illustrated in Fig. 8 (g). Looking at Fig. 8 (g), the power factor of the DFIG in this operating case is almost unity power factor, thus the reactive power Q_g is almost equal zero in the period. The active power P_g is generated to the grid but during the fault period from 100ms to 250ms the active power P_g is reduced to zero. However, after the fault is cleared the active power P_g is gradually increased to the normal value. Therefore, the experimental results and the grid connection code as shown in Fig. 6 confirm that the LVRT capability of the DFIG test system is still connected to the grid.

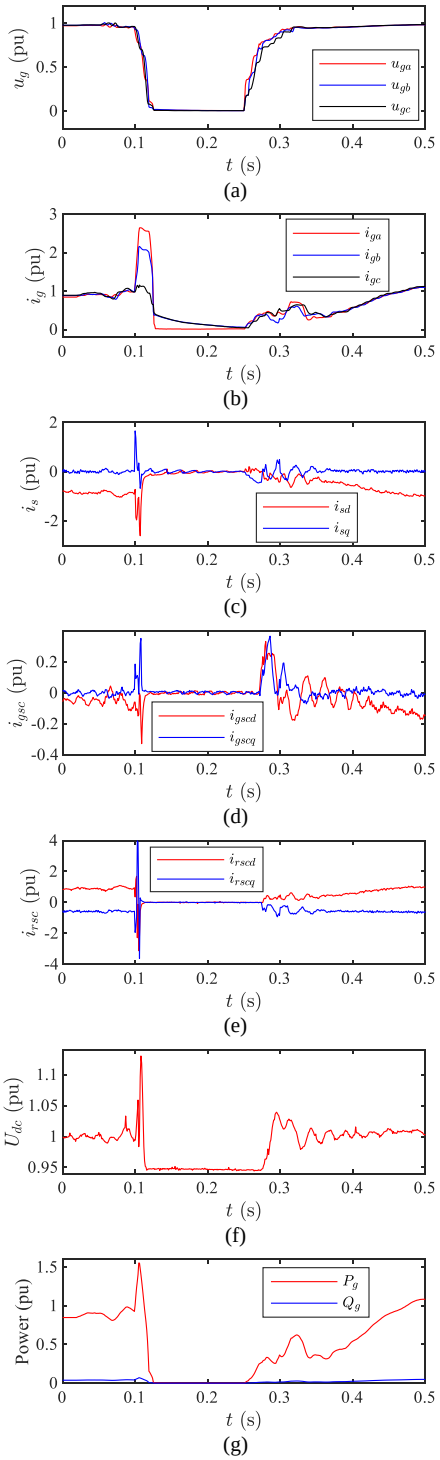

Fig. 8. The three-phase voltage dip: (a) Grid voltage, (b) Grid current, (c) Stator current, (d) GSC current, (e) RSC current, and (f) DC-link voltage, (g) Active and reactive power.

Based on the 0.8kW DFIG experimental system in the laboratory, many experiments with different wind speeds are carried out to validate the performance of LVRT capability of the DFIG under the sub-synchronous and super-synchronous operation modes. At the wind speed of 12.5m/s the DFIG is operated in the synchronous operation which is performed in the previous study case. By observing the response of the DFIG system operating with the wind speeds when a balanced voltage dip occurred, the experimental results are synthesized in Table II.

TABLE II: THE EXPERIMENTS FOR DIFFERENT WIND SPEED MODE TO TEST LVRT CAPABILITY

Wind speed mode	Wind speed (m/s)	Fault duration (ms)				
		100	150	200	250	300
Sub-synchronous operation speed	10.0	✓	✓	×	×	×
	10.5	✓	✓	×	×	×
	11.0	✓	✓	×	×	×
	11.5	✓	✓	×	×	×
	12.0	✓	✓	×	×	×
Synchronous operation speed	12.5	✓	✓	×	×	×
Super-synchronous operation speed	13.0	✓	×	×	×	×
	13.5	✓	×	×	×	×
	14.0	✓	×	×	×	×
	14.5	✓	×	×	×	×

Note: "✓" represents for the DFIG connected to the grid; "×" represents for the DFIG disconnected to the grid.

B. Test Under Unbalanced Voltage Dip Condition

Fig. 9 shows a single-phase due to a single-phase to ground fault with 100% of the grid at the PCC side by using the grid emulator happens at a time duration of 150ms starting 50ms. It shows clearly that the phase-c voltage is reduced to zero in the fault time duration from 100ms to 250ms. In this case, the grid current i_g is recorded and shown in Fig. 9 (b) for evaluating the LVRT capability of the DFIG test system. Based on the figures, the phase-a and phase-b currents are increased but the phase-b current is decreased in the fault stage from 100ms to 250ms. At the time of 250ms, the fault is ended the grid voltage u_g is recovered to the nominal value, therefore the grid current i_g is the comeback to the normal value as the pre-fault stage. In addition, the responses in the GSC and RSC controllers including the stator current i_s, the GSC current i_{gsc}, and the RSC current i_{rsc} under for the above fault are shown in Fig. 9 (c), Fig. 9 (d), and Fig. 9 (e), respectively. In these figures, the red line indicates the *d*-component of the current and the blue line indicates the *q*-component. Moreover, the DC-link voltage between the GSC and RSC has shown in Fig. 9 (f) confirms that it is almost stable in the fault stage from 100ms to 250ms. Fig. 9 (g) illustrates the active and reactive behavior of the DFIG system. Based on these experimental results for this case, we can see that the DFIG test system is still connected to the grid and it still generates power to the grid in normal operating mode.

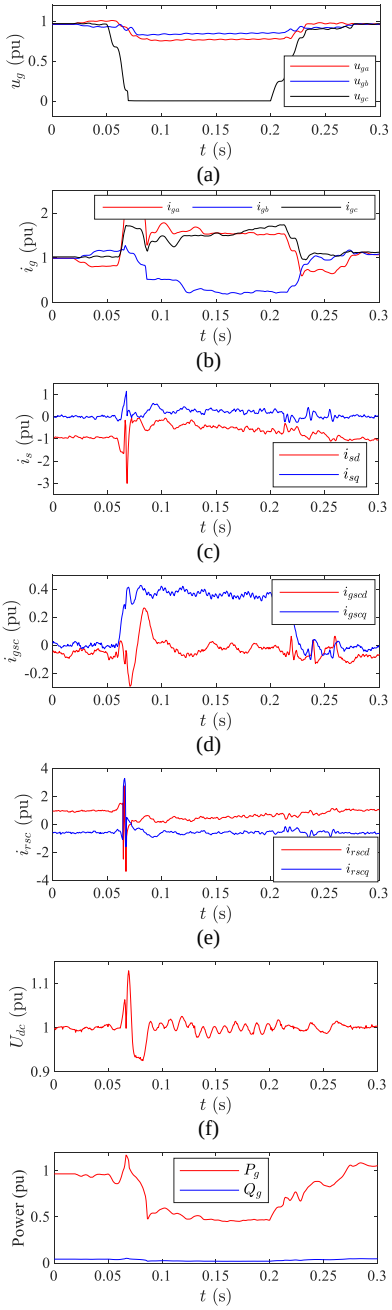

Fig. 9. Single-phase to ground fault: (a) Grid voltage, (b) Grid current, (c) Stator current, (d) GSC current, (e) RSC current, (f) DC-link voltage, (g) Active and reactive power.

Fig. 10 shows another test of unbalanced voltage dip condition that a phase-to-phase fault with 100% of the grid at the PCC side by using the grid emulator happens at a time duration of 150ms starting 50ms. It is clear from Fig. 10 (a) that the voltage magnitude of phase-b is normal but the voltage magnitudes of phase-a and phase-c are reduced to zero in the fault stage from 100ms to 250ms. Because of this voltage dip, the three-phase grid currents i_g are varied when the fault happens as shown in Fig. 10 (b). In the fault stage from 100ms to 250ms, the RMS grid currents of phase-a and phase-b are increased. Then they come back to nominal value when the fault ended at the time of 250ms as shown in Fig. 10 (b). For this case, the *d*-component and *q*-component of the stator,

the GSC controller, and the RSC controller are recorded and plotted in Fig. 10 (c), Fig. 10 (d), and Fig. 10 (e), respectively. It is clear from these figures, there is a variation in the *d*-component, and *q*-component around the starting time at 100ms and the ending time at 250ms of the fault. Moreover, the DC-link voltage U_{dc} shown in Fig. 10 (f) is almost unchanged during the time duration of the voltage dip from 100ms to 250ms. It has only a large variation around the starting time at 100ms. Fig. 10 (g) shows the active and reactive behavior of the DFIG system. Therefore in these experimental cases, the LVRT capability of the DFIG test system is still connected to the grid according to the grid connection code as shown in Fig. 6.

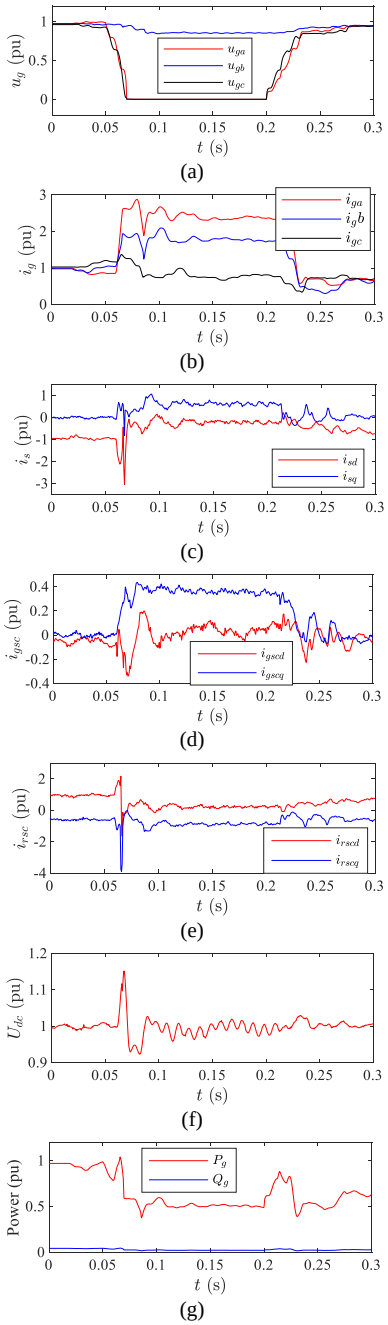

Fig. 10. The phase-to-phase fault: (a) Grid voltage, (b) Grid current, (c) Stator current, (d) GSC current, (e) RSC current, (f) DC-link voltage, (g) Active and reactive power.

VI. Conclusion

The electric-wind experimental configuration, using the doubly-fed induction generator (DFIG), had been introduced in this paper. The low voltage ride through (LVRT) capability was carried out to study for this configuration. The main parts, composing of the wind turbine, rotor-side converter, grid-side converter, chopper, and crowbar, were used in this configuration. Especially, the wind turbine and gearbox were replaced by the servo motor. To emulate a grid fault in the network, a grid emulator was used in the testing workbench. The LVRT requirement in the German grid code was verified to analyze and validate the proposed electric-wind system under the balanced and unbalanced sag condition tests. The obtained experimental results show that the complete architecture of DFIG-WECS can be applied for the engineer training course in the field of renewable energy conversion in the university's laboratory to study with LVRT capability.

Conflict of Interest

The authors declare no conflict of interest.

Author Contributions

All authors conducted the research; Ngo Minh Khoa and Doan Duc Tung conducted the experiments in the laboratory. Ngo Minh Khoa and Le Van Dai wrote the paper; all authors had approved the final version.

References

[1] S. Muller, M. Deicke, and R. W. De Doncker, "Doubly fed induction generator systems for wind turbines," *IEEE Industry Applications Magazine*, vol. 8, no. 3, pp. 26-33, 2002.

[2] Y. Song and F. Blaabjerg, "Overview of DFIG-based wind power system resonances under weak networks," *IEEE Trans. Power Electronics*, vol. 32, no. 6, pp. 4370-4394, 2016.

[3] B. Wu, Y. Lang, N. Zargari, and S. Kouro, *Power Conversion and Control of Wind Energy Systems*, John Wiley & Sons, 2011.

[4] J. A. Baroudi, V. Dinavahi, and A. M. Knight, "A review of power converter topologies for wind generators," *Renewable Energy*, vol. 32, no. 14, pp. 2369-2385, 2007.

[5] Z. Chen, J. M. Guerrero, and F. Blaabjerg, "A review of the state of the art of power electronics for wind turbines," *IEEE Trans. Power Electronics*, vol. 24, no. 8, pp. 1859-1875, 2009.

[6] F. Blaabjerg, M. Liserre, and K. Ma, "Power electronics converters for wind turbine systems," *IEEE Trans. Industry Applications*, vol. 48, no. 2, pp. 708-719, 2011.

[7] D. Xu, F. Blaabjerg, W. Chen, and N. Zhu, *Advanced Control of Doubly Fed Induction Generator for Wind Power Systems*, John Wiley & Sons, 2018.

[8] M. I. Mosaad, "Comparative study between the electrical generators used in wind energy conversion systems," *International Journal of Energy*, vol. 14, pp.88-92, 2020.

[9] M. Tsili and S. Papathanassiou, "A review of grid code technical requirements for wind farms," *IET Renewable Power Generation*, vol. 3, no. 3, pp. 308-332, 2009.

[10] O. P. Mahela, N. Gupta, M. Khosravy, and N. Patel, "Comprehensive overview of low voltage ride through methods of grid integrated wind generator," *IEEE Access*, vol. 7, pp. 99299-99326, 2019.

[11] J. Morren and S. W. De Haan, "Ridethrough of wind turbines with doubly-fed induction generator during a voltage dip," *IEEE Trans. Energy Conversion*, vol. 20, no. 2, pp. 435-441, 2005.

[12] T. Sun, Z. Chen, and F. Blaabjerg, "Voltage recovery of grid-connected wind turbines after a short-circuit fault," in *Proc. 29th Annual Conference of the IEEE Industrial Electronics Society*, Roanoke, VA, USA, Nov. 2003.

[13] Y. Zhou, P. Bauer, J. A. Ferreira, and J. Pierik, "Operation of grid-connected DFIG under unbalanced grid voltage condition," *IEEE Trans. Energy Conversion*, vol. 24, no. 1, pp. 240-246, 2009.

[14] J. Lopez, P. Sanchis, X. Roboam, and L. Marroyo, "Dynamic behavior of the doubly fed induction generator during three-phase voltage dips," *IEEE Trans. Energy Conversion*, vol. 22, no. 3, pp. 709-717, 2007.

[15] F. K. Lima, A. Luna, P. Rodriguez, E. H. Watanabe, and F. Blaabjerg, "Rotor voltage dynamics in the doubly fed induction generator during grid faults," *IEEE Trans. Power Electronics*, vol. 25, no. 1, pp. 118-130, 2009.

[16] X. Kong, Z. Zhang, X. Yin, and M. Wen, "Study of fault current characteristics of the DFIG considering dynamic response of the RSC," *IEEE Trans. Energy Conversion*, vol. 29, no. 2, pp. 278-287, 2014.

[17] B. Qin, H. Li, X. Zhou, J. Li, and W. Liu, "Low-voltage ride-through techniques in DFIG-based wind turbines: A review," *Applied Sciences*, vol. 10, no. 6, p. 2154, 2020.

[18] M. Rahimi and M. Parniani, "Low voltage ride-through capability improvement of DFIG-based wind turbines under unbalanced voltage dips," *International Journal of Electrical Power Energy Systems*, vol. 60, pp. 82-95, 2014.

[19] P. Jayanthi and D. Devaraj, "Enhancement of LVRT capability in grid connected wind energy systems using crowbar," in *Proc. IEEE International Conference on Clean Energy and Energy Efficient Electronics Circuit for Sustainable Development*, Krishnankoil, India, Dec. 2019.

[20] C. Raghavendran, J. P. Roselyn, and D. Devaraj, "Development and performance analysis of intelligent fault ride through control scheme in the dynamic behaviour of grid connected DFIG based wind systems," *Energy Reports*, vol. 6, pp. 2560-2576, 2020.

[21] H. Dong, H. Wu, J. Pan, Y. Chen, and B. Xu, "Research on double-fed induction generator low voltage ride through based on double braking resistors using fuzzy control," *Energies*, vol. 11, no. 5, p. 1155, 2018.

[22] R. Liu, J. Yao, X. Wang, P. Sun, J. Pei, and J. Hu, "Dynamic stability analysis and improved LVRT schemes of DFIG-based wind turbines during a symmetrical fault in a weak grid," *IEEE Trans. Power Electronics*, vol. 35, no. 1, pp. 303-318, 2019.

[23] S. Swain and P. K. Ray, "Ride-through capability improvement of a grid-integrated DFIG based wind turbine system using a new protection design," in *Proc. 6th IEEE International Conference on Power Systems*, New Delhi, India, March 2016.

[24] L. V. Dai, X. Li, Y. Li, T. L. T. Dong, and L. C. Quyen, "An innovative control strategy to improve the fault ride-through capability of DFIGs based on wind energy conversion systems," *Energies*, vol. 9, no. 2, p. 69, 2016.

[25] X. Yang, G. Liu, A. Li, and L. V. Dai, "A predictive power control strategy for DFIGs based on a wind energy converter system," *Energies*, vol. 10, no. 8, p. 1098, 2017.

[26] M. I. Mosaad, A. Alenany, and A. Abu-Siada, "Enhancing the performance of wind energy conversion systems using unified power flow controller," *IET Generation, Transmission and Distribution*, vol. 14, no. 10, pp. 1922-1929, 2020.

[27] M. I. Mosaad, A. Abu-Siada, and M. F. El-Naggar, "Application of superconductors to improve the performance of DFIG-based WECS," *IEEE Access*, vol. 7, no. 1, pp. 103760-103769, 2019.

[28] S. Hu and H. Xu, "Experimental research on LVRT capability of DFIG WECS during grid voltage sags," in *Proc. Asia-Pacific Power and Energy Engineering Conference*, Chengdu, China, March 2010.

[29] T. Long, S. Shao, P. Malliband, M. Mathekga, E. Abdi, R. McMahon, and P. Tavner, "Experimental LVRT performance of a 250 kW brushless DFIG," in *Proc. European Wind Energy Conference and Exhibition*, 2012.

[30] M. K. Döşoğlu, "A new approach for low voltage ride through capability in DFIG based wind farm," *International Journal of Electrical Power Energy Systems*, vol. 83, pp. 251-258, 2016.

[31] G. Wen, Y. Chen, Z. Zhong, and Y. Kang, "Dynamic voltage and current assignment strategies of nine-switch-converter-based DFIG wind power system for low-voltage ride-through (LVRT) under symmetrical grid voltage dip," *IEEE Trans. Industry Applications*, vol. 52, no. 4, pp. 3422-3434, 2016.

[32] S. Seman, J. Niiranen, and A. Arkkio, "Ride-through analysis of doubly fed induction wind-power generator under unsymmetrical network disturbance," *IEEE Trans. Power Systems*, vol. 21, no. 4, pp. 1782-1789, 2006.

[33] G. Byeon, I. K. Park, and G. Jang, "Modeling and control of a doubly-fed induction generator (DFIG) wind power generation system for real-time simulations," *Journal of Electrical Engineering Technology*, vol. 5, no. 1, pp. 61-69, 2010.

[34] F. Blaabjerg, *Control of Power Electronic Converters and Systems*, Academic Press, vol. 2, 2018.

[35] X. Zhen, Z. Xing, Y. Shuying, L. Qin, and Z. Wenfeng, "Study on control strategy of maximum power capture for DFIG in wind turbine system," in *Proc. 2nd International Symposium on Power Electronics for Distributed Generation Systems*, Hefei, China, June 2010.

[36] L. V. Dai and D. D. Tung, "Modeling for development of simulation tool: A case study of grid-connected doubly fed induction generator based on wind energy conversion system," *International Journal of Applied Engineering Research*, vol. 12, no. 11, pp. 2981-2996, 2017.

[37] B. H. Chowdhury and S. Chellapilla, "Double-fed induction generator control for variable speed wind power generation," *Electric Power Systems Research*, vol. 76, no. 9, pp. 786-800, 2006.

[38] G. Abad, J. Lopez, M. Rodriguez, L. Marroyo, and G. Iwanski, *Doubly Fed Induction Machine: Modeling and Control for Wind Energy Generation*, John Wiley & Sons, 2011.

[39] J. Han, Z. Liu, and N. Liang, "Nonlinear adaptive robust control strategy of doubly fed induction generator based on virtual synchronous generator," *IEEE Access*, vol. 8, pp. 159887-159896, 2020.

Ngo Minh Khoa received the M.Sc. degree and the Ph.D. degree in Electrical Engineering both from The University of Danang - University of Science and Technology, Vietnam, in 2010 and 2017, respectively. He has been a lecturer at Faculty of Engineering and Technology, Quy Nhon University since 2006. His current research interests include power system stability, power quality improvement, renewable energy, and smart grid.

Doan Duc Tung received the M.Sc. degree and the Ph.D. degree in Electrical Engineering both from Hanoi University of Science and Technology, Vietnam, in 2004 and 2009, respectively. He has been a lecturer at Faculty of Engineering and Technology, Quy Nhon University since 2000. He became an Associate Professor in 2019. He is currently a Vice Rector of Quy Nhon University. His research interests include electric machine, renewable energy, and optimization methods.

Le Van Dai received the M.Sc. degree in electrical engineering from the Ho Chi Minh City University of Technology, Vietnam in 2008. He received the Ph.D. degree in information and electricity engineering from Hunan University, Changsha, China in 2016. He has been a lecturer of the Faculty of Electrical Engineering, Industrial University of Ho Chi Minh City, Vietnam since 2011. His current research interests include FACTS control, solar PV energy conversion, control of wind power generation, and grid integration.